Title

Engineered metal oxide nanomaterials inhibit corneal epithelial wound healing in vitro and in vivo

Authors

Kim, Soohyun

Gates, Brooke

Leonard, Brian C

et al.

Publication Date

2020

DOI

10.1016/j.impact.2019.100198

Peer reviewed

HHS Public Access

Author manuscript

NanoImpact. Author manuscript; available in PMC 2021 January 01.

Published in final edited form as:

NanoImpact. 2020 January ; 17: . doi:10.1016/j.impact.2019.100198.

Engineered metal oxide nanomaterials inhibit corneal epithelial wound healing *in vitro* and *in vivo*

Soohyun Kim[a], **Brooke Gates**[a], **Brian C. Leonard**[a], **Megan Gragg**[a], **Kent E. Pinkerton**[b], **Laura Van Winkle**[b,d], **Christopher J. Murphy**[a,c], **Georgios Pyrgiotakis**[e], **Zhenyuan Zhang**[e], **Philip Demokritou**[e], **Sara M. Thomasy**[a,c,*]

[a]Department of Surgical and Radiological Sciences, School of Veterinary Medicine, University of California - Davis, Davis, CA, 95616, USA;

[b]Center for Health and the Environment, University of California - Davis, Davis, CA, 95616, USA;

[c]Department of Ophthalmology and Vision Science, School of Medicine, University of California - Davis, Davis, CA, 95616, USA;

[d]Department of Anatomy, Physiology and Cell Biology, School of Veterinary Medicine, University of California - Davis, Davis, CA, 95616, USA;

[e]Center for Nanotechnology and Nanotoxicology, HSPH-NIEHS Nanosafety Center, Department of Environmental Health, Harvard T.H. Chan School of Public School, Harvard University, 665 Huntington Boston, MA 02115, USA.

Abstract

Ocular exposure to metal oxide engineered nanomaterials (ENMs) is common as exemplified by zinc oxide (ZnO), a major constituent of sunscreens and cosmetics. The ocular surface that includes the transparent cornea and its protective tear film are common sites of exposure for metal ENMs. Despite the frequency of exposure of the ocular surface, there is a knowledge gap regarding the effects of metal oxide ENMs on the cornea in health and disease. Therefore, we studied the effects of metal oxide ENMs on the cornea in the presence or absence of injury. Cell viability of immortalized human corneal epithelial (hTCEpi) cells was assessed following treatment with 11 metal oxide ENMs with a concentration ranging from 0.5 to 250 μg/mL for 24 hours. An epithelial wound healing assay with a monolayer of hTCEpi cells was then performed using 11 metal oxide ENMs at select concentrations based on data from the viability assays. Subsequently, based on the *in vitro* results, *in vivo* testing of precorneal tear film (PTF) quantity and stability as well as a corneal epithelial wound healing were tested in the presence or absence ZnO or vanadium pentoxide (V_2O_5) at a concentration of 50 μg/mL. We found that WO_3, ZnO, V_2O_5 and CuO ENMs significantly reduced hTCEpi cell viability in comparison to vehicle control

*Corresponding author: Tel: +1 530 752 0926, Fax: +1 530 752 3708, smthomasy@ucdavis.edu.

Conflict of interest

The authors declare no conflict of interest.

or the other metal oxide ENMs tested. Furthermore, ZnO and V_2O_5 ENMs also significantly decreased hTCEpi cell migration. Although ZnO and V_2O_5 did not alter PTF parameters of rabbits *in vivo*, corneal epithelial wound healing was significantly delayed by topical ZnO while V_2O_5 did not alter wound healing. Finally, hyperspectral images confirmed penetration of ZnO and V_2O_5 through all corneal layers and into the iris stroma. Considering the marked epithelial toxicity and corneal penetration of ZnO, further investigations on the impact of this ENM on the eye are warranted.

Keywords

metal oxide engineered nanomaterials; nanometals; corneal epithelium; corneal wound healing; nanotoxicity

1. Introduction

Metal oxide engineered nanomaterials (ENMs) are commonly used in various industrial applications and daily consumer goods including sunscreens (Burnett and Wang, 2011), cosmetic products (Lu et al., 2015), antimicrobial coatings (Raghunath and Perumal, 2017), solar cells (Singh et al., 2016), semiconductors (Jo et al., 2015), pigments and UV-absorption filters (Singh and Nanda, 2014; Kim and Min, 2013), filling materials in food production (Kapoor et al., 2018), as well as toothpastes, and sanitary ware coatings (Contado, 2015). In spite of the widely publicized benefits of metal oxide ENMs, recent concerns have been raised regarding potential adverse effects of these ENMs on human health and the environment. The toxicity of metal oxide ENMs is primarily attributed to overproduction of reactive oxygen species (ROS) induced by ENMs and ROS-induced damage (Djurišić et al., 2015; Raghupathi et al., 2011). However, other mechanisms of toxicity exist including release of metal ions (Martín-Cameán et al., 2015; De Matteis et al., 2015), the internalization of nanomaterials into the cells, and cell membrane disorganization due to accumulation of nanomaterials on the cell surface (Raghupathi et al., 2011; Li et al., 2008). A myriad of factors may impact the putative toxicity of metal oxide ENMs, including exposure dose and time, solvent pH, and oxidation/reduction potential (Joo and Zhao, 2017).

Inhalation and dermal routes of exposure are especially prominent for gases, aerosols and liquid particles of metal oxide ENMs (Yah et al., 2012) The eye, particularly the cornea, experiences similar exposure as dermal and inhalation routes. Although it is difficult to determine what constitutes risk for the eye, lungs and skin following metal oxide ENM exposure, each exposed organ can have an adverse response and the response may differ depending on the tissue type. Little is known regarding what kind of risks metal oxide ENM exposure poses for the eye. Yet, some metal oxide ENMs are used in commercial sunscreens and cosmetics (Burnett et al., 2011; Liu et al., 2012) that are routinely applied in close proximity to the eye thus increasing the potential for ocular exposure. Traditionally, ZnO and TiO_2 are major ingredients of sunscreens because of their ability to block ultraviolet light. Since 1999, the Food and Drug Administration have allowed the use of nanoparticles (NPs) in sunscreen, subsequently a large number of these products were formulated with nano-sized ZnO or TiO_2 (Australian Government TGA, 2006; Newman et al., 2009).

Specifically, >6,000 tons of sunscreens produced annually contain these NPs (Australian Government TGA, 2006). Given that facial sunscreens and cosmetics are commonly used, there is great potential for direct exposure to the ocular surface. A recent article by Zhou and colleagues demonstrated that ZnO decreased corneal epithelial cell viability and migration *in vitro* (Zhou et al., 2014). We therefore hypothesized that metal oxide ENMs that displayed *in vitro* epithelial toxicity, including ZnO, could also delay corneal epithelial wound healing *in vivo*.

The precorneal tear film (PTF) covers the ocular surface and serves as the first functional barrier by diluting and slowing the penetration of any exogenous material that contacts the eye via reflex tearing, blinking and drainage through the nasolacrimal duct (Kaur and Kanwar, 2002). Significant alterations of the PTF can lead to ocular surface diseases and delayed corneal epithelial wound healing (Rolando and Zierhut, 2001). The cornea is the outermost, transparent layer of the eye that provides protection for the fragile inner structures and it is in direct contact with the external environment. It can be viewed as a trilaminar sandwich comprised of a multilayered epithelium, a stroma and a single-layer endothelium with its specialized extracellular matrix. The corneal epithelium is self-renewing through proliferation of the stem cells located predominantly at the limbus and that give rise to basal cells that subsequently differentiate to intermediate polygonal wing cells and ultimately superficial squamous cells that are sloughed into the tears (Lu et al., 2001). Tight junctions between these squamous epithelial cells act as a physical barrier to prevent the entrance of noxious foreign agents (Urtti, 2006). Furthermore, the cornea also protects against mechanical trauma with a specific healing process for each layer. The corneal epithelium must repair quickly to prevent infection of, and damage to, the deeper layers. As such, the cells from the wound margin rapidly respond with flattening and centripetal migration to cover the defect followed by proliferation and differentiation of basal cells to restore the layers of the epithelium (Bukowiecki et al., 2017). Experimental corneal epithelial wounds can be easily created by mechanical (Li et al., 2017) or chemical methods (Ghiasi et al., 2018) then monitored non-invasively and in real time *in vivo*. As such, the unique attributes of the corneal epithelium offer numerous advantages for investigating the interaction of nanomaterials with *in vivo* tissues.

Currently, there are a paucity of studies assessing the impact of metal oxide ENMs on corneal cell health *in vitro* (Zhou et al., 2014) and *in vivo* (Han et al., 2017). Therefore, we tested the viability and migration of corneal epithelial cells *in vitro* following exposure to 11 metal oxide ENMs of commercial relevance including aluminum oxide (Al_2O_3), iron(III) oxide (Fe_2O_3), cerium(IV) oxide (CeO_2), copper(II) oxide (CuO), magnesium(IV) oxide (MgO), tungsten(VI) oxide (WO_3), vanadium(V) oxide (V_2O_5), titanium(IV) oxide (TiO_2) and zinc(II) oxide (ZnO) ENMs. Based on the *in vitro* results, we then tested the impact of topical ZnO as well as V_2O_5 ENMs on PTF quantity and stability, and corneal epithelial wound healing *in vivo* using a rabbit model.

MATERIALS AND METHODS

ENM synthesis and characterization and preparation of suspensions

The following metal oxide and gold ENMs were assessed in this study (primary particle diameter in parenthesis): Au (15 nm), Al_2O_3 (30 nm), CeO_2 (10 and 30 nm), CuO (50 nm), Fe_2O_3 (10 nm), MgO (20 nm), TiO_2 (100 nm), TiO_2 (25 nm), WO_3 (15 nm), ZnO (50 nm) and V_2O_5 (100 nm). The ENMs used in this study were procured, synthesized, and characterized by the Engineered Nanomaterials Coordination Core (ERCC) as part of the Nanotechnology Health Implications Research (NHIR) Consortium at the Harvard T.H. Chan School of Public Health. Specifically, the citrate-capped Au nanoparticles were synthesized following the Turkevich method and characterized by Dong and coworkers (Dong et al., 2019). The CuO, TiO_2 (100 nm), TiO_2 (25 nm), MgO, ZnO, and V_2O_5 were procured by Sigma Aldrich, Precheza, Acros Organics, Strem Chemicals, Inc., Meliorum Technologies, Inc. and NanoShel LLC, respectively. The physicochemical and biological characteristics of CuO and ZnO have been presented by Eweje and colleagues (Eweje et al., 2019) while the 100 nm and 25 nm of TiO_2 have been described by Lee *et al.* (2018) and Ahn *et al.* (2018), respectively. The Al_2O_3, CeO_2, Fe_2O_3, MgO, and WO_3 nanoparticles were synthesized via flame spray pyrolysis using the Harvard Versatile Engineered Nanomaterials Generation System (VENGES) (Demokritou et al., 2010). Details on the synthesis and characterization of Al_2O_3, CeO_2, and Fe_2O_3 have been presented by Beltran-Huarac and coworkers (Beltran-Huarac et al., 2018) and characterized by ERCC. Details on the synthesis of WO_3 is presented in Supplement A. Finally, the physicochemical and biological properties of pristine MgO, V_2O_5, and WO_3 nanoparticles are summarized in Supplementary tables 1,2 and 3. It is important to note that all particles used in this study presented a near-spherical shape with the exception of V_2O_5, which was in the form of a nanoflake. Primary particle diameters as measured by transmission electron microscopy and specific surface area as measured by the Brunauer-Emmett-Teller (BET) method are summarized in Supplement B.

Prior to the use of the EMNs in this experiment, resuspended ENMs were sonicated using a calibrated sonication system (2510R-MT; Branson Ultrasonic Co., Danbury, CT) following the protocol reported by DeLoid and coworkers (DeLoid et al., 2017). Briefly, each ENM was placed into a 15-ml conical tube and deionized water (DW) added to achieve a final concentration of 2.5 mg/ml. Next, the nanosuspensions were vortexed at high speed for 30 seconds and sonicated for ~3–6 minutes as calculated time for each material (Supplement C). Following sonication, the stock suspensions were vortexed again for at least 30 seconds at high speed and diluted with balanced salt solution (BSS; Alcon®, Fort Worth, Texas) or culture media to the final concentration. All diluted suspensions were used immediately after preparation and all preparation procedures were repeated every 24 hours. Stability of metal oxide nanomaterials in suspension was tested with dynamic light scattering (DLS). The hydrodynamic diameter and polydispersity index were measured using a DLS instrument (Zetasizer Nano S90, Malvern Instruments Ltd., Malvern, UK) at 1 and 24 h after preparation. (Supplement C).

Cell culture

Human telomerase reverse transcriptase-immortalized corneal epithelial (hTCEpi) cells, graciously donated by James Jester, PhD (University of California Irvine), were used between passage 48 and 56. The hTCEpi cells were cultured in growth medium composed of EpiLife® (LifeTechnologies, Carlsbad, CA) supplemented with 1% EpiLife Defined Growth Supplement (EDGS®; a proprietary combination of bovine serum albumin, bovine transferrin, hydrocortisone, recombinant human-like growth factor type-1, prostaglandin, and recombinant human epidermal growth factor; Life Technologies) and 1% penicillin-streptomycinamphotericin B (HyCloneTM 100X; HyClone, Logan, UT) at 37°C and 5% CO_2.

Viability assays

The effects of 11 metal oxide ENMs on the viability of hTCEpi cells were tested using MTT (3-[4,5-dimethylthiazol-2-yl]-2,5 diphenyl tetrazolium bromide) and Calcein-AM (acetoxymethyl ester) assays. The hTCEpi cells were plated into 96-well plates at a density of 7,000 cells per well in 100 μL culture medium and allowed to attach for 24 hours prior to treatment. Then, cells were treated for 24 hours with one of 11 metal oxide ENMs at concentrations between 0.05 to 250 μg/mL in six replicates. Citrate capped gold NPs (Au NP; 5 μg/mL), and an equal volume of DW to the treatment volume of the ENM suspensions were used as negative and vehicle controls, respectively; saponin (1 mg/mL) was used as positive control. Then, MTT (0.5 mg/mL) solution was added to each well and incubated for 4 h at 37°C. The culture medium supernatant was carefully aspirated from the wells without disturbing the formazan precipitate. The formazan crystals were dissolved in 50 μL/well with dimethyl sulphoxide (DMSO; Sigma Chemical Co., St. Louis, MO) and mixed thoroughly. The absorbance was measured at 540 nm using a microplate spectrophotometer (Synergy 4; BioTek, Instruments Inc., Winooski, VT).

Cell viability was also tested using the Calcein-AM Cell Viability Kit (TREVIGEN®, R&D Systems, Inc. Minneapolis, MN). Viable hTCEpi cells were fluorescently labeled by Calcein-AM (1 μM for 30 minutes) following a 24 hour incubation with one of the aforementioned metal oxide ENMs, Au NP, DW or saponin (1 mg/mL) as described previously. The fluorescence intensity was measured with a 490 nm excitation filter and a 520 nm emission filter using a microplate spectrophotometer (Synergy 4). All viability tests were performed in triplicate; absorbance of ENMs only without cells at the aforementioned concentrations were also measured as a blank control for both assays. Then, the absorbed values for each concentration of NPs tested with MTT and Calcein-AM assays (ENMs only without cells) were subtracted from the original values (ENMs with cells) for the final calculation to control for any impact of ENMs on the viability measurement, These values were normalized to the vehicle control, and final results were expressed as percentage viability relative to the vehicle control.

In vitro cell migration assay

In vitro cell migration was measured using the Oris™ 96-well cell migration assay kit (Platypus Technologies, Madison, WI) as per the manufacturer's instructions. In brief, 7×10^4 cells/ml of hTCEpi cells were seeded in each well of the 96-well plate, which had a

stopper in middle of each well, and allowed to attach for 24 hours in 37 °C. Once the cells formed a confluent monolayer, the silicone stoppers were removed to allow cells to migrate into the detection zone. Concomitantly, the cells were treated with one metal oxide ENM at selected concentrations for each material based on the viability assay results; five concentrations of each ENM were utilized including the lowest concentration with a demonstrated significant decrease in cell viability. The hTCEpi cells were also treated with DW or cytochalasin D (1 μg/mL) as vehicle or positive controls, respectively. Twenty-four hours after initiation of the migration, cells were fixed with 4% paraformaldehyde in PBS (Thermo Fisher Scientific Chemicals Inc., Waltham, MA) for 30 minutes. Nuclei were stained for 10 mins at room temperature with 4',6-diamidino-2-phenylindole (DAPI; BioGenex, San Ramon, CA) 1:5000 in PBS. Cells were imaged immediately after staining using a fluorescence microscope with x 5 objective (Axiovert 200 M; Carl Zeiss, Jena, Germany) or x 4 objective (BZ-X800; Keyence Co., Osaka, Japan). The area devoid of cells was measured using ImageJ analysis software (version 1.421). Data were expressed as relative percent migration compared with the vehicle control (DW).

Animals

Eighteen female New Zealand White rabbits (Charles River laboratories, Wilmington, MA) were used with a mean age of 4.0 ± 0.0 months and body weight of 3.38 ± 0.19 kg. Animals were divided into three groups with the following treatments: (1) BSS (vehicle control; n=6), (2) 50 μg/mL of ZnO NP suspension (n=6), and (3) 50 μg/mL of V_2O_5 nanoflake suspension (n=6); treatments were given 6 times daily in both eyes (oculus uterque, OU). The study was approved by the Institutional Animal Care and Use Committee of the University of California, Davis (IACUC #19691) and performed in compliance with the Association of Research in Vision and Ophthalmology statement for the use of animals in vision research. A complete ophthalmic examination and imaging were performed prior to inclusion in the study; only animals free of ocular disease were used.

Test article preparation and treatments

For the *in vivo* study, the highest tolerated dose (~0.5 μg/mL) of the ZnO and V_2O_5 ENMs was selected based on the *in vitro* toxicity and migration assays and multiplied by 100-fold (50 μg/mL) for use as a topical treatment to be administered six times daily while considering the following factors: (1) immediate dilution of the 40 μL ENM suspension by the PTF present on the ocular surface, and (2) exposure time on the corneal surface that the ENM suspensions will likely reside on the ocular surface after topical application. All treatment articles were prepared daily prior to initial treatment. A stock solution of ZnO or V_2O_5 ENMs at a concentration of 2.5 mg/mL in DW was sonicated for 4 minutes following vigorous vortexing for 30 seconds. Following sonication, the ZnO and V_2O_5 stock suspensions were vortexed again for 30 seconds prior to use. Subsequently, the stock solutions were diluted in BSS to a final concentration 50 μg/mL and 600 μL each aliquoted in 1.5-ml microcentrifuge tubes; the aliquots were stored at 4°C until use and vortexed 30 seconds immediately prior to use. Forty μL of ZnO or V_2O_5 ENMs or vehicle controls were topically administered 6 times daily OU.

Evaluation of PTF

Both eyes of 18 healthy rabbits were used to assess the tear film at baseline and 7 days following treatment. Tear film thickness and tear meniscus height, depth and area were assessed by Fourier-domain optical coherence tomography (FD-OCT, Optovue Inc., Fremont, CA). Specifically, 3 FD-OCT images were taken using the CAM-S (S/N 30107; 3-mm scan length) lens, and tear film thickness at the central cornea was measured using the RTVue 100 software (version 6.1, Optovue Inc.) (Supplement D). For analysis of the tear meniscus, three 45°, 8-mm length line scan images were obtained with the CAM-L (S/N 40107; 8-mm scan length) in a perpendicular position at the center of the inferior eyelid margin, and then its height, depth and area were measured using the RTVue 100 software (Supplement D). To access aqueous tear secretion, a Schirmer tear test (STT)-1 was performed by placing a commercially available standardized sterile test strip (Merck Animal Heath, Summit, NJ) within the ventral conjunctival fornix for one minute. Tear film break-up time (TFBUT) was measured applying 2 μL of 2% sodium fluorescein solution that was diluted with BSS from 10% sodium fluorescein (AK-FLOUR®; Akron Inc., Lake Frost, IL).

Epithelial debridement

At day 8 after initiating treatment, rabbits were pre-medicated with midazolam (0.7 mg/kg, intramuscular injection (IM)) and hydromorphone (0.1 mg/kg, IM) followed by ketamine (10–30 mg/kg, IM) for induction and maintenance of anesthesia. The surgical area was prepped with 0.2% povidone iodine and saline. The central 8-mm of the corneal epithelium of the right eye (OD) was marked with a trephine prior to application of 0.5% proparacaine hydrochloride ophthalmic solution (Alcon laboratories, Inc., Fort Worth, TX). Then, the marked area was debrided using a blunt spatula (Excimer Spatula; Beaver-Visitec, Waltham, MA) and epithelium confirmed to be absent from the area of the wound with fluorescein stain (NaFL ophthalmic strip; BIO GLOTM; 1 mg, HUB Pharmaceuticals, LLC., Rancho Cucamonga, CA). The cornea was imaged with a digital camera (Nikon D300, Nikon co., Tokyo, Japan ; flash 1/4, iso 250, F11; with cobalt blue filters [Blue-AWB, Nikon] over flash and yellow filter [HMC 62mm Y[K2], HOYA] over lens) to establish wound area at baseline.

Atropine 1% (Atropine Sulfate Ophthalmic Solution 1%; Akorn, Inc., Lake Forest, IL) and ofloxacin 0.3% (Alcon, Hunengerg, Switzerland) ophthalmic solutions were administered OD following the epithelial debridement five minutes apart, then, artificial tear ointment (Rugby Laboratories, Inc., Duluth, GA) was applied OU five minutes later to prevent the drying of the corneal surface. Buprenorphine (0.03–0.06 mg/kg, IM) was administered to reverse the hydromorphone and to provide analgesia. All animals were monitored every 10 minutes until they returned to an upright body position.

Ocular exam scoring, imaging, and image analysis

A complete ophthalmic examination was performed prior to and daily following surgery until the integrity of the corneal epithelium had been re-established in the vehicle control group as determined by the absence of fluorescein retention. The semiquantitive preclinical ocular toxicology scoring (SPOTS) system (Eaton et al., 2017) was used in this study to assess the anterior segment using a hand-held slit lamp biomicroscope (SL-15). Rebound

tonometry was performed to measure intraocular pressure (TonoVet; Icare, Helsinki, Finland). Fluorescein stain was applied to assess epithelial wound area twice daily with digital photography (Nikon D300). All images were analyzed using image analysis software (ImageJ; ver 1.51j8; National Institutes of Health, Bethesda, MD). The percent remaining wound area at each time point was calculated from the photographic images using the following equation:

$$\% \text{ Wound area} = \text{Wound area on day X/Wound area on day } 0 \times 100$$

Tissue harvest, processing and hyperspectral microscopy

Rabbits were euthanized with pentobarbital (200 mg/kg, IV) at 4 days post-surgery when the corneal epithelial wounds were completely healed in the control group. To identify the presence and spatial location of ENMs, enucleated eyes were fixed in 10% neutral buffered formalin and underwent routine paraffin processing. A 5 μm thick paraffin-embedded section from each eye with the greatest limbal diameter was dissolved in xylene for 10 mins twice and rinsed in 100% ethanol for 5 mins twice. Then, a coverslip was applied and bound to the surface with mounting media (VectaMountTM Permanent Mounting Medium; Vector Laboratories, Inc., Burlingame, CA). The ZnO or V_2O_5 ENM suspensions (50 μg/mL in BSS) were used as positive controls. Hyperspectral microscopy was performed to detect ZnO and V_2O_5 ENMs using a high signal-to-noise, darkfield-based illumination on an Olympus BX-41 microscope (Cytoviva, Auburn, AL; 10x and 40x). Spectral profiles from individual particles within the corneal layers were compared with the particles of the positive controls. When the spectral profile of the selected particle is congruous to the profile of the control ENM, the selected particle was considered a match with that ENM.

Statistical Analysis

Data were presented as mean ± standard deviation (SD) and statistical analysis was performed with GraphPad Prism 7.03 (GraphPad Software Inc., San Diego, CA). Data sets were compared with Students *t*-test with Welch's correction, Kruskal-Wallis test (nonparametric oneway ANOVA) followed by Dunn's multiple comparisons test or repeated measures two-way ANOVA followed by Tukey's multiple comparisons as indicated. Values of $P < 0.05$ were considered statistically significant. To compare *in vitro* toxicities for different concentrations of V_2O_5 nanoflake and ZnO NP, repeated measure two-way ANOVA with the Geisser-Greenhouse correction followed by the Sidak's multiple comparisons test. Two-way ANOVA followed by Sidak's multiple comparisons tests was performed to compare the *in vitro* cell migrations between V_2O_5 nanoflake and ZnO NP at different concentrations.

RESULTS

Most ENMs did not agglomerate in suspension at 24 hours

The properties of metal oxide ENM suspensions in EpiLife® media or BSS was measured by DLS. The mean hydrodynamic diameter of the 11 metal oxide EMNs were 100–1700 nm with < 0.7 polydispersity index (Supplement C). The hydrodynamic diameters of each metal

oxide ENM did not significantly differ between 1- and 24-hours post suspension, indicating particle size distribution did not change significantly over 24 h of suspension ($P > 0.05$).

V_2O_5, WO_3, and ZnO ENMs markedly decreased cell viability

For the 11 metal oxide ENMs tested, the data generated from the MTT and Calcein AM assays were remarkably consistent (Figure 1). While Al_2O_3, CeO_2 (10 and 30 nm), CuO, Fe_2O_3, and MgO ENMs significantly decreased hTCEpi cell viability at the highest concentrations tested (100 and/or 250 μg/mL) in one or both assays, only V_2O_5, WO_3, and ZnO ENMs significantly decreased cell viability at concentrations of 50 μg/mL or less in both assays. The V_2O_5 and ZnO ENMs were highly toxic at lower concentrations with cell viabilities markedly less than controls at 12.5 and 5 μg/mL, respectively. When comparing the V_2O_5 and ZnO ENMs, the ZnO NPs were significantly more toxic than the V_2O_5 nanoflakes in the concentration range of 5 to 50 μg/ml ($P = 0.008$ for 5 μg/ml and $P < 0.001$ for 12.5, 25 and 50 μg/ml).

Low concentrations of ZnO and V_2O_5 ENMs significantly decreased cell migration

Cell migration *in vitro* was significantly delayed for Al_2O_3, CeO_2 (10 nm), CuO and Fe_2O_3 ENMs at ≥ 50 μg/ml, CeO_2 (30 nm) and TiO_2 (25 nm) ENMs at ≥ 100 μg/ml, and TiO_2 (100 nm) ENM at 250 μg/ml; MgO and WO_3 ENMs did not significantly delay hTCEpi cell migration at the concentrations tested versus vehicle control (Figure 2). By contrast, V_2O_5 and ZnO ENMs showed markedly reduced migration rates at ≥ 5 μg/mL. In particular, the ZnO NPs had significantly lower migration rates compared to the V_2O_5 nanoflakes at three of the concentrations tested ($P = 0.002$ for 0.5 μg/ml and $P < 0.001$ for 5 and 12.5 μg/ml). Based on the aforementioned cell viability and these migration assay results *in vitro*, ZnO and V_2O_5 ENMs were selected to test their impact on the corneal epithelium in health and following wounding *in vivo*.

ZnO and V_2O_5 ENMs showed no effects to the PTF

No significant differences were observed between ENM treated groups (ZnO or V_2O_5) and vehicle controls in terms of aqueous tear production, TFBUT, tear meniscus thickness, tear meniscus height, volume, and area ($P > 0.05$); no differences were also observed in these parameters prior to or following 7 days of treatment with ENMs or vehicle ($P > 0.05$; Table 1).

Corneal epithelial wound healing was significantly delayed by topical ZnO NP in vivo

Corneal epithelial wound sizes were measured using digital images of sodium fluorescein staining (Figure 3A). The 50% wound closure was achieved within 27.0, 35.5 and 27.8 hours post-wounding in the BSS, ZnO NP and V_2O_5 nanoflake treated groups, respectively. All wounded corneas were completely healed by 96 hours post wounding in the BSS and V_2O_5 nanoflake treated groups. By contrast, half of the animals in the ZnO NP group still had a corneal ulcer at 96 hours post wounding, and 2 of 6 corneas in the ZnO NP group were not healed at the final time point (105 hours post wounding). Compared to vehicle control and V_2O_5 nanoflake treatment, the ZnO NP treated group showed significantly delayed wound healing rates from 33 to 81 hours post wounding (Figure 3B); no significant differences

between the V_2O_5 nanoflake treated group and vehicle control were identified at any time point.

Conjunctival hyperemia and swelling, discharge, corneal opacity and iris hyperemia were transiently observed in all wounded eyes until re-epithelialization but no significant differences were observed between groups using SPOTS (data not shown). In unwounded eyes, no significant adverse effects were observed in ZnO NP or V_2O_5 nanoflake groups versus vehicle control at any time point.

Transcorneal penetration of ZnO and V_2O_5 ENMs

Hyperspectral darkfield microscopy demonstrated transcorneal penetration of ZnO and V_2O_5 ENMs in both wounded and unwounded eyes with deposition in the corneal epithelium, stroma, Descemet's membrane and endothelium; a few particles of ZnO were also observed in the iris stroma (Figure 4).

DISCUSSION

In the present study, we documented a spectrum of *in vitro* toxicity as measured by epithelial cell viability and migration of 11 metal oxide ENMs at concentrations ranging between 0.5 to 250 μg/mL. Specifically, we determined that ZnO and V_2O_5 ENMs inhibited cell viability as well as delayed *in vitro* epithelial migration at markedly lower concentrations (~5 μg/mL) than other materials. We then demonstrated that 50 μg/mL of ZnO NPs but not V_2O_5 nanoflakes delayed epithelial wound repair *in vivo* in a rabbit model. Commercial sunscreen products contain up to 25%w/w (generally between 10–20 %w/w) of ZnO NPs with an ~60–120 μg/mL of exposure to ZnO NPs following a single application to human skin (Surekha et al., 2012). Therefore, the concentration of ZnO NP tested in this *in vivo* study is consistent with potential physiologic exposure of these NPs at the ocular surface.

Previous studies have found that metal oxide ENMs exhibit relatively high toxicity compared to bulk metals through abundant dissolution of metal ions (Jeong et al., 2018), internalization into mammalian cells (Karisson et al., 2014; Noventa et al., 2018), and increased generation of reactive oxygen species (ROS) (Horie et al., 2012). In particular, ZnO NPs are highly soluble and release relatively large amounts of zinc ions (Zn^{2+}) not only in the extracellular environment but also into the cells following uptake (Karisson et al., 2014; Cronholm et al., 2013; Ghaemi et la., 2018). Nanosized ZnO can also generate ROS which induces DNA damage and cytotoxicity via UV-induced photocatalysis (Li et al., 2012; Guo et al., 2013). Therefore, it is unsurprising that ZnO NP demonstrated the greatest toxicity *in vitro* and *in vivo* to corneal epithelial cells in the present study. Consistent with these results, numerous studies have determined that ZnO NPs are markedly cytotoxic to a variety cell types including corneal limbal epithelial cells (Zhou et al., 2014), bronchial epithelial cells (Heng et al., 2010), intestinal epithelial cells (Setyawati et al., 2015), retinal ganglion cells (Guo et al., 2013), retinal photoreceptors (Guo et al., 2015), periodontal fibroblasts (Seker et al., 2014), and corneal fibroblasts (Zhou et al., 2014). Similar to its cytotoxic effects to mammalian cells, ZnO NPs are potent antibacterial agents with a wide spectrum of bacteriostatic properties (Sirelkhatim et al., 2015) as well as show inhibitory activity to several fungal species including Fusarium species (Sharma et al., 2010).

We also identified reduced epithelial cell viability *in vitro* following exposure to V_2O_5 nanoflakes albeit less marked than that of ZnO NPs. Vanadium compounds are generally acutely toxic to most species via a myriad of exposure routes including inhalation, and ingestion (Gruzewska et al., 2014). Moreover, the toxicity increases with its oxidation state, with the pentavalent forms causing the most harmful effects (Korbecki et al., 2012; Wilk et al., 2017). In particular, V_2O_5 causes DNA damage via oxidation (Ehrlich et al., 2008) and induces pulmonary inflammation via excessive secretion of chemokines (Fallahi et al., 2018). While ocular irritation has been reported as a clinical feature of workplace exposure to V_2O_5 (Venkataraman and Sudha, 2005), studies investigating the effects of V_2O_5 ENMs to the eye are lacking. Interestingly, topical application of V_2O_5 nanoflakes (50 μg/mL) six times daily did not impair corneal epithelial wound healing or incite ocular irritation in rabbits in the present study despite delaying epithelial migration and cytotoxicity *in vitro*, albeit less markedly that the ZnO NPs. We confirmed that the V_2O_5 nanoflakes accumulated in the cornea by hyperspectral darkfield-based microscopy indicating that the epithelial cells were exposed to the V_2O_5 nanoflakes. Cell migration is an orchestrated process that involves sequential formation and dissolution of adhesions between cells and to the extracellular matrix (ECM), cytoskeletal remodeling, mechanical forces and signaling networks (Le Clainche and Carlier, 2008; Tang and Geriach, 2017). Unlike *in vivo* corneal epithelial repair, the *in vitro* cell migration assay is carried out with only a monolayer of cells in the absence of critical ECM and inflammatory signals found *in vivo*. In aggregate, the *in vitro* and *in vivo* data from the ZnO and V_2O_5 ENMs suggests that metal oxide cytotoxicity is variable and ENMs displaying marked *in vitro* toxicity must be confirmed using *in vivo* models.

Nanomaterials can impede cell migration by changing cellular mechanical properties and force generation (Jain and Matsumura, 2016). In particular, ROS which is commonly generated by metal oxide ENMs, can affect cell migration through microtubule remodeling (Apopa et al., 2009). In the present study, most metal oxide ENMs tended to decrease corneal epithelial cell migration in a dose-dependent manner with the exception of MgO and WO_3 NPs, which did not impact cellular migration at all concentrations tested. Magnesium ions promote the integrin-mediated cell migration of melanoma cells (Maier et al., 2004) and enhance infiltration of osteoblasts by increasing cell motility (Kim et al., 2017). These observations may be a possible explanation why the MgO NP had a negligible impact on migration of corneal epithelial cells *in vitro*. To our knowledge, this is the first assessment of the impact of WO_3 NPs on cell migration. In particular, ZnO NP dramatically inhibited cell migration rates at concentrations > 5 μg/mL *in vitro* consistent with previous reports using human corneal fibroblasts, human corneal limbal epithelial cells (Zhou et al., 2014) and a murine photoreceptor-derived cell line (Guo et al., 2015). To our knowledge, this is the first study to demonstrate that topical application of ZnO NPs to the eye delays corneal epithelial wound healing *in vivo*. The ZnO NPs may delay epithelial wound healing by increasing tumor necrotic factor-α, interleukin (IL)-6, and IL-8 production (Faddah et al., 2012) or by inhibiting mitochondrial function by the Zn^{2+} cation release (Xia et al., 2008). Although ZnO has been used topically for management of skin wounds, its effects to the wound closure time is controversial (Lansdown et al., 2007). Interestingly, various skin wound dressing materials containing ZnO NPs accelerated wound healing in *in vivo* mouse dermal

wounds despite the ZnO NPs demonstrating toxicity to these cells in the *in vitro* environment (Lu et al., 2017). Given that ZnO NPs are a major component of numerous sunscreens and cosmetics (Australian Government TGA, 2006), and their use is expanding for skin wound dressings due to their potent antimicrobial effects (Lansdown et al., 2007; Lu et al., 2017), further studies are warranted to identify the mechanisms by which ZnO NPs delay corneal epithelial wound healing.

We also performed a comprehensive assessment of the PTF following a 7-day topical application of ZnO and V_2O_5 ENMs to heathy rabbit eyes. Dry eye disease is a prevalent condition amongst aged adults with an overall economic burden of ~$55 billion in the United States (Yu et al., 2011a). It is a multifactorial disorder that is characterized by PTF instability with concomitant ocular surface inflammation, irritation and vision compromise (Nelson et al., 2017). Moreover, a normal PTF is also critical to appropriate corneal wound healing (Rolando and Zierhut, 2001). Metal oxide ENMs have never been studied within the context of dry eye disease and yet their ubiquitous nature in the environment suggest that they may have a profound impact on the PTF with downstream effects on ocular tissues including the cornea. For example, Yu and coworkers have reported robust induction of mucin production in murine airways by V_2O_5 via the NF-κB pathway (Yu et al., 2011b). Mucin is a critical component of the PTF to maintain the stability of the PTF and protecting the epithelial barrier of the ocular surface (Hodges and Dartt, 2013). Cell surface associated mucins, such as MUC1 and −16, reduce epithelial permeability by forming a dense glycocalyx that covers the apical surface of the cornea and conjunctiva. (Argüeso et al., 2009). Thus, it is critical to continue investigating how ENMs impact the PTF to gain a comprehensive understanding of the effects of ENMs on the ocular surface and during corneal epithelial wound repair.

Potential toxicity concerns of ENMs in cosmetics and sunscreens result from their ability to evade immunologic defense mechanisms and to induce inflammatory responses (Australian Government TGA, 2006). It is well known that both ZnO and V_2O_5 ENMs can induce inflammation in other body systems (Australian Government TGA, 2006; Fallahi et al., 2018). Therefore, the ability of metal oxide ENMs to penetrate through the cornea into the anterior chamber is critical to the potential intraocular toxicity of these ENMs. Indeed, we demonstrated ZnO NPs in the iris stroma following topical application to the eye in the present study. This also raises concerns about the impact of cumulative exposure to NPs that an individual human may experience over a lifetime. Many studies have reported that penetration of ZnO NPs in skin is limited to the stratum corneum, the outermost layer of the skin and composed with ~20 layers of dead cells with tight junctions and intercellular junctions (Newman et al., 2009). However, skin with a compromised stratum corneum may not present an effective barrier to penetration of the ENMs (van der Merwe et al., 2009). For example, ZnO NPs (20 nm; 75–360 mg/kg) passed through skin with a compromised stratum corneum in rats (Surekha et al., 2012) and other studies demonstrated increased concentrations of Zn in the internal organs of mice following short term dermal application of sunscreen containing ZnO NPs (~30 nm; average of 0.1 g/animal) (Osmond-McLeod et al., 2014). In this study, we confirmed that the topically applied ZnO NPs, as well as the V_2O_5 nanoflakes, penetrated through and accumulated in all corneal layers of both wounded

and nonwounded eyes indicating that the eye may be at greater risk for toxicity following exposure versus the skin.

In conclusion, ZnO ENMs showed the most marked toxicity *in vitro* to corneal epithelial cells amongst 11 metal oxide ENMs tested and significantly delayed corneal epithelial wound healing in a rabbit. Considering the high exposure risk of ZnO to the ocular surface, further investigations on the mechanisms by which ZnO NPs delay corneal epithelial repair and its effects on corneal stromal wound healing are warranted.

Supplementary Material

Refer to Web version on PubMed Central for supplementary material.

Acknowledgements

Research reported in this publication was supported by the National Institute of Environmental Health Sciences of the National Institutes of Health under Award Number NIEHS U01 ES027288 as part of the Nanotechnology Health Implications Research (NHIR) Consortium. The content is solely the responsibility of the authors and does not necessarily represent the official views of the National Institutes of Health. The engineered nanomaterials used in the research presented in this publication have been procured/developed, characterized, and provided by the Engineered Nanomaterials Resource and Coordination Core established at Harvard T. H. Chan School of Public Health (NIH grant # U24ES026946) as part of the Nanotechnology Health Implications Research Consortium. The CytoViva Hyperspectral imaging system was supported by a NIH shared equipment grant S10 OD021789 and the histopathology processing was supported by NIH National Eye Institute P30 EY12576.

References

Ahn S, Ardona HAM, Lind JU, Eweje F, Kim SL, Gonzalez GM, Liu Q, Zimmerman JF, Pyrgiotakis G, Zhang Z, Beltran-Huarac J, Carpinone P, Moudgil BM, Demokritou P, Parker KK, 2018 Mussel-inspired 3D fiber scaffolds for heart-on-a-chip toxicity studies of engineered nanomaterials. Anal. Bioanal. Chem 410(24), 6141–6154. [PubMed: 29744562]

Apopa PL, Qian Y, Shao R, Guo NL, Schwegier-Berry D, Pacurari M, Porter D, Shi X, Vallyathan V, Castranova V, Flynn DC, 2009 Iron oxide nanoparticles induce human microvascular endothelial cell permeability through reactive oxygen species production and microtubule remodeling. Part Fibre. Toxicol 6, 1. [PubMed: 19134195]

Argüeso P.l., Guzman-Aranguez A, Mantelli F, Cao Z, Ricciuto J, Panjwani N, 2009 Association of cell surface mucins with galectin-3 contributes to the ocular surface epithelial barrier. J. Biol. Chem 284(34), 23037–23045. [PubMed: 19556244]

Australian Government TGA, 2006 OTC medication section: A review of the scientific literature on the safety of nanoparticulate titanium dioxide or zinc oxide in sunscreens Available from:http://www.tga.gov.au/npmeds/sunscreen-zotd.pdf.

Beltran-Huarac J, Zhang Z, Pyrgiotakis G, DeLoid G, Vaze N, Hussian SM, Demokritou P, 2018 Development of reference metal and metal oxide engineered nanomaterials for nanotoxicology research using high throughput and precision flame spray synthesis approaches. NanoImpact 10, 26–37. [PubMed: 30035243]

Bukowiecki A, Hos D, Cursiefen C, Eming SA, 2017 Wound-healing studies in cornea and skin: parallels, differences and opportunities. Int. J. Mol. Sci 18(6), pii: E1257. [PubMed: 28604651]

Burnett ME, Wang SQ, 2011 Current sunscreen controversies: a critical review.Photodermatol. Photoimmunol. Photomed 27(2), 58–67. [PubMed: 21392107]

Contado C, 2015 Nanomaterials in consumer products: a challenging analytical problem. Front Chem 3, 48. [PubMed: 26301216]

Cronholm P, Karisson HL, Hedgerg J, Lowe TA, Winnberg L, Elihn K, Wallinder IO, Möller L, 2013 Intracellular uptake and toxicity of Ag and CuO nanoparticles: a comparison between nanoparticles and their corresponding metal ions. Small 9(7), 970–982. [PubMed: 23296910]

De Matteis V, Malvindi MA, Galeone A, Brunetti V, De Luca E, Kote S, Kshirsaga P, Sabella S, Bardi G, Pompa PP, 2015 Negligible particle-specific toxicity mechanism of silver nanoparticles: the role of Ag+ ion release in the cytosol. Nanomedicine 11(3), 731–739. [PubMed: 25546848]

DeLoid GM, Cohen JM, Pyrgiotakis G, Demokritou P, 2017 Preparation, characterization, and in vitro dosimetry of dispersed, engineered nanomaterials. Nat. Protoc 12(2), 355–371 [PubMed: 28102836]

Demokritou P, Buchel R, Molina RM, Deloid GM, Brain JD, Pratsinis SE., 2010 Development and characterization of a versatile engineered nanomaterial generation system (VENGES) suitable for toxicological studies. Inhal. Toxicol 22 Suppl 2, 107–116. [PubMed: 20701428]

Djurišić AB, Leung YH, Ng AM, Xu XY, Lee PK, Degger N, Wu RS, 2015 Toxicity of metal oxide nanoparticles: mechanisms, characterization, and avoiding experimental artefacts. Small 11(1), 26–44. [PubMed: 25303765]

Dong J, Carpinone PL, Pyrgiotakis G, Demokritou P, Moudgil BM, 2019 Synthesis of precision gold nanoparticles using turkevich method. KONA Powder and Particle Journal, Published online 24 August 2019. [Doi; 10.14356/kona.2020011]

Eaton JS, Miller PE, Bentley E, Thomasy SM, Murphy CJ, 2017 The SPOTS system: an ocular scoring system optimized for use in modern preclinical drug development and toxicology. J. Ocul. Pharmacol. Ther 33(10), 718–734. [PubMed: 29239680]

Ehrlich VA, Nersesyan AK, Atefie K, Hoelzl C, Ferk F, Bichler J, Valic E, Schaffer A, Schulte-Hermann R, Fenech M, Wagner KH, Knasmüller S, 2008 Inhalative exposure to vanadium pentoxide cause DNA damage in workers: results of a multiple end point study. Environ. Health Perspect 116(12), 1689–1693. [PubMed: 19079721]

Eweje F, Ardona HAM, Zimmerman JF, O'Connor BB, Ahn S, Grevesse T, Rivera KN, Bitounis D, Demokritou P, Parker KK, 2019 Quantifying the effects of engineered nanomaterials on endothelial cell architecture and vascular barrier integrity using a cell pair model. Nanoscale 11(38), 17878–17893. [PubMed: 31553035]

Faddah LM, Abdel Baky NA, Al-Rasheed NM, Al-Rasheed NM, Fatani AJ, Atteya M, 2012 Role of quercetin and arginine in ameliorating nano zinc oxide-induced nephrotoxicity in rats. BMC Complement Altern. Med 12, 60. [PubMed: 22551254]

Fallahi P, Foddis R, Elia G, Ragusa F, Patrizio A, Guglielmi G, Frenzilli G, Benvenga S, Cristaudo A, Antonelli A, Ferrari SM, 2018 Induction of Th1 chemokine secretion in dermal fibroblasts by vanadium pentoxide. Mol. Med. Rep 17(5), 6914–6918. [PubMed: 29532885]

Ghaemi B, Shaabani E, Nanafi-Taher R, Jafari Nodooshan S, Sadeghpour A, Kharrazi S, Amani A, 2018 Intracellular ROS induction by Ag@ZnO corne-shell nanoparticles: frontiers of permanent optically active holes in breast cancer theranostic. ACS Appl. Mater. Interfaces 10(29), 24370–24381. [PubMed: 29932633]

Ghiasi Z, Gray T, Tran P, Dubielzig R, Murphy C, McCartney DL, Reid TW, 2018 The effect of topical substance-P plus insulin-like growth factor-1 (IGF-1) on epithelial healing after photorefractive keratectomy in rabbits. Transl. Vis. Sci. Technol 7(1), 12.

Gruzewska K, Michno A, Pawelczyk T, Bielarczyk H, 2014 Essentiality and toxicity of vanadium supplements in health and pathology. J. Physiol. Pharmacol 65(5), 603–611. [PubMed: 25371519]

Guo D, Bi H, Liu B, Wu Q, Wang D, Cui Y, 2013 Reactive oxygen species-induced cytotoxic effects of zinc oxide nanoparticles in rat retinal ganglion cells. Toxicol. In Vitro 27(2), 731–738. [PubMed: 23232460]

Guo DD, Li QN, Li CM, Bi HS, 2015 Zinc oxide nanoparticles inhibit murine photoreceptor- derived cell proliferation and migration via reducing TGF- β and MMP- 9 expression in vitro. Cell Prolif 48, 198–208. [PubMed: 25615023]

Han JY, Kang B, Eom Y, Kim HM, Song JS, 2017 Comparing the effects of particulate matter on the ocular surfaces of normal eyes and a dry eye rat model. Cornea 36(5), 605–610 [PubMed: 28306598]

Heng BC, Zhao X, Xiong S, Ng KW, Boey FY, Loo JS, 2010 Toxicity of zinc oxide (ZnO) nanoparticles on human bronchial epithelial cells (BEAS-2B) is accentuated by oxidative stress. Food Chem. Toxicol 48(6), 1762–1766. [PubMed: 20412830]

Hodges RR, Dartt DA, 2013 Tear film mucins: front line defenders of the ocular surface; comparison with airway and gastrointestinal tract mucins. Exp. Eye Res 117, 62–78. [PubMed: 23954166]

Horie M, Kato H, Fujita K, Endoh S, Iwahashi H, 2012 In vitro evaluation of cellular response induced by manufactured nanoparticles. Chem. Res. Toxicol 25(3), 605–619. [PubMed: 22136515]

Jain M, Matsumura K, 2016 Polyampholyte- and nanosilicate-based soft bionanocomposites with tailorable mechanical and cell adhesion properties. J. Biomed. Mater. Res. A 104(6), 1379–1386. [PubMed: 26833827]

Jeong J, Kim SH, Lee S, Lee DK, Han Y, Jeon S, Cho WS, 2018 Differential contribution of constituent metal ions to the cytotoxic effects of fast-dissolving metal-oxide nanoparticles. Front Pharmacol 9, 15. [PubMed: 29403385]

Jo JW, Kim J, Kim KT, Kang JG, Kim MG, Kim KH, Ko H, Kim J, Kim YH, Park SK, 2015 High stable and imperceptible electronics utilizing photoactivated heterogeneous solgel metal-oxide dielectrics and semiconductors. Adv. Mater 27(7), 1182–1188. [PubMed: 25580710]

Joo SH, Zhao D, 2017 Environmental dynamics of metal oxide nanoparticles in heterogenous systems: A review. J. Hazard Mater 322(Pt A), 29–47. [PubMed: 26961405]

Kapoor V, Phan D, Pasha ABMT, 2018 Effects of metal oxide nanoparticles on nitrification in wastewater treatment systems: A systematic review. J. Environ. Sci. Health. A. Tox. Hazard Subst. Environ. Eng 53(7), 659–668.

Karisson HL, Gliga AR, Calléja FM, Gonçalves CS, Wallinder IO, Vrieling H, Fadeel B, Hendriks G, 2014 Mechanism-based genotoxicity screening of metal oxide nanoparticles using the ToxTracker panel of reporter cell lines. Part Fibre. Toxicol 11, 41. [PubMed: 25179117]

Kaur IP, Kanwar M, 2002 Ocular preparations: the formulation approach. Drug Dev. Ind. Pharm 28(5), 473–493. [PubMed: 12098838]

Kim KJ, Choi S, Sang Cho Y, Yang SJ, Cho YS, Kim KK, 2017 Magnesium ions enhance in filtration of osteoblasts in scaffolds via increasing cell motility. J. Mater. Sci. Mater. Med 28(6), 96. [PubMed: 28508951]

Kim YK, Min DH, 2013 UV protection of reduced graphene oxide films by TiO2 nanoparticle incorporation. Nanoscale 5(9), 3638–3642. [PubMed: 23532399]

Korbecki J, Baranowska-Bosiacka I, Gutowska I, Chlubek D, 2012 Biochemical and medical importance of vanadium compounds. Acta Biochim. Pol 59(2), 195–200. [PubMed: 22693688]

Lansdown AB, Mirastschijski U, Stubbs N, Scanlon E, Agren MS, 2007 Zinc in wound healing: theoretical, experimental, and clinical aspects. Wound Repair Regen 15(1), 2–16. [PubMed: 17244314]

Le Clainche C, Carlier MF, 2008 Regulation of actin assembly associated with protrusion and adhesion in cell migration. Physiol. Rev 88(2), 489–513. [PubMed: 18391171]

Lee JY, Wang H, Pyrgiotakis G, DeLoid GM, Zhang Z, Beltran-Huarac J, Demokritou P, Zhong W, 2018 Analysis of lipid adsorption on nanoparticles by nanoflow liquid chromatography-tandem mass spectrometry. Anal. Bioanal. Chem 410(24), 6155–6164. [PubMed: 29845324]

Li Q, Mahendra S, Lyon DY, Brunet L, Liga MV, Li D, Alvarez PJ, 2008 Antimicrobial nanomaterials for water disinfection and microbial control: potential applications and implications. Water Res 42(18), 4591–4602. [PubMed: 18804836]

Li S, Zhou J, Bu J, Ning K, Zhang L, Li J, Guo Y, He X, He H, Cai X, Chen Y, Reinach PS, Liu Z, Li W, 2017 Ectodysplasin A protein promotes corneal epithelial cell proliferation. J. Biol. Chem 292(32), 13391–13401. [PubMed: 28655773]

Li Y, Zhang W, Niu J, Chen Y, 2012 Mechanism of photogenerated reactive oxygen species and correlation with the antibacterial properties of engineered metal-oxide nanoparticles. ACS Nano 6(6), 5164–5173. [PubMed: 22587225]

Liu S, Jones L, Gu FX, 2012 Nanomaterials for ocular drug delivery. Macromol. Biosci 12(5), 608–620. [PubMed: 22508445]

Lu L, Reinach PS, Kao WWY, 2001 Corneal epithelial wound healing. Exp. Biol. Med 226(7), 653–664.

Lu PJ, Huang SC, Chen YP, Chiueh LC, Shih DY, 2015 Analysis of titanium dioxide and zinc oxide nanoparticles in cosmetics. J. Food. Drug. Anal 23(3), 587–594. [PubMed: 28911719]

Lu Z, Gao J, He Q, Wu J, Liang D, Yang H, Chen R, 2017 Enhanced antibacterial and wound healing activities of microporous chitosan-Ag/ZnO composite dressing. Carbohydr. Polym 156, 460–469. [PubMed: 27842847]

Martín-Cameán A, Jos Á, Mellado-García P, Iglesias-Linares A, Solano E, Cameán AM, 2015 In vitro and in vivo evidence of the cytotoxic and genotoxic effects of metal ions released by orthodontic appliances: A review. Environ. Toxicol. Pharmacol 40(1), 86–113. [PubMed: 26093195]

Maier JA, Bernardini D, Rayssiguier Y, Mazur A, 2004 High concentrations of magnesium modulate vascular endothelial cell behavior in vitro. Biochim. Biophys. Acta 1689(1), 6–12. [PubMed: 15158908]

Nelson JD, Craig JP, Akpek EK, Azar DT, Belmonte C, Bron AJ, Clayton JA, Dogru M, Dua HS, Foulks GN, Gomes JAP, Hammitt KM, Holopainen J, Jones L, Joo CK, Liu Z, Nichols JJ, Nichols KK, Novack GD, Sangwan W, Stapleton F, Tomlinson A, Tsubota K, Willcox MDP, Wolffsohn JS, Sullivan DA, 2017 TFOS DEWS II introduction. Ocul. Surf 15(3), 269–275. [PubMed: 28736334]

Newman MD, Stotland M, Ellis JI, 2009 The safety of nanosized particles in titanium dioxide- and zinc oxide-based sunscreens. J. Am. Acad. Dermatol 61(4), 685–692. [PubMed: 19646780]

Noventa S, Rowe D, Galloway T, 2018 Mitigating effect of organic matter on the in vivo toxicity of metal oxide nanoparticles in the marine environment. Environ. Sci.: Nano 5, 1764–1777.

Osmond-McLeod MJ, Oytam Y, Kirby JK, Gomez-Fernandez L, Baxter B, McCall MJ, 2014 Dermal absorption and short-term biological impact in hairless mice from sunscreens containing zinc oxide nano- or large particles. Nanotoxicology 8 Suppl 1, 72–84.

Pierscionek BK, Li Y, Schachar RA, Chen W, 2012 The effect of high concentration and exposure duration of nanoceria on human lens epithelial cells. Nanomedicine 8(3), 383–390. [PubMed: 21722619]

Prow T, Smith JN, Grebe R, Salazar JH, Wang N, Kotov N, Lutty G, Leary J, 2006 Construction, gene delivery, and expression of DNA tethered nanoparticles. Mol. Vis 12, 606–615. [PubMed: 16760897]

Raghunath A, Perumal E, 2017 Metal oxide nanoparticles as antimicrobial agents: a promise for the future. Int. J. Antimicrb. Agents 49(2), 137–152.

Raghupathi KR, Koodali RT, Manna AC, 2011 Size-dependent bacterial growth inhibition and mechanism of antibacterial activity of zinc oxide nanoparticles. Langmuir 27(7), 4020–4028. [PubMed: 21401066]

Righettoni M, Tricoli A, Pratsinis SE, 2010a WO3 sensors for highly selective detection of acetone for easy diagnosis of diametes by breath analysis. Analytical Chemistry 82(9), 3581–3587. [PubMed: 20380475]

Righettoni M, Tricoli A, Pratsinis SE, 2010b Thermally stable, silica-doped ε-WO3 for sensing of acetone in the human breath. Chemistry of Materials 22(10), 3152–3157.

Rolando M, Zierhut M, 2001 The ocular surface and tear film and their dysfunction in dry eye disease. Surv. Ophthalmol 45 Suppl 2, S203–210 [PubMed: 11587144]

Seker S, Elçin AE, Yumak T, Sınağ A, Elçin YM, 2014 In vitro cytotoxicity of hydrothermally symthesized ZnO nanoparticles on human periodontal ligament fibroblast and mouse dermal fibroblast cells. Toxicol. In Vitro 28(8), 1349–1358. [PubMed: 25016134]

Setyawati MI, Tay CY, Leong DT, 2015 Mechanistic investigation of the biological effects of SiO_2, TiO_2, and ZnO nanoparticles on intestinal cells. Small 11(28), 4358–3468.

Singh P, Nanda A, 2014 Enhanced sun protection of nano- sized metal oxide particles over conventional metal oxide particles: An in vitro comparative study. Int. J. Cosmet. Sci 36(3), 273–283. [PubMed: 24575878]

Singh T, Singh J, Miyasaka T, 2016 Role of metal oxide electron-transport layer modification on the stability of high performing perovskite solar cells. ChemSusChem 9(18), 2559–2566. [PubMed: 27554065]

Sirelkhatim A, Mahmud S, Seeni A, Kaus NHM, Ann LC, Bakhori SKM, Hasan H, Mohamad D, 2015 Review on zinc oxide nanoparticles: antibacterial activity and toxicity mechanism. Nanomicro Lett 7(3), 219–242. [PubMed: 30464967]

Sharma D, Rajput J, Kaith BS, Kaur M, Sharma S, 2010 Synthesis of ZnO nanoparticles and study of their antibacterial and antifungal properties. Thin Solid Films 519(3), 1224–1229

Surekha P, Kishore AS, Srinivas A, Selvam G, Goparaju A, Reddy PN, Murthy PB, 2012 Repeated dose dermal toxicity study of nano zinc oxide with Sprague-Dawley rats. Cutan. Ocul. Toxicol 31(1), 26–32. [PubMed: 21830917]

Tang DD, Geriach BD, 2017 The roles and regulation of the actin cytoskeleton, intermediate filaments and microtubules in smooth muscle cell migration. Respir. Res 18(1), 54. [PubMed: 28390425]

Urtti A, 2006 Challenges and obstacles of ocular pharmacokinetics and drug delivery. Adv. Drug Deliv. Rev 58(11), 1131–1135 [PubMed: 17097758]

van der Merwe D, Tawde S, Pickrell JA, Erickson LE, 2009 Nanocrystalline titanium dioxide and magnesium oxide in vitro dermal absorption in human skin. Cutan. Ocul. Toxicol 28(2), 78–82. [PubMed: 19514931]

Venkataraman BV, Sudha S, 2005 Vanadium toxicity. Asian J. Exp. Sci 19(2), 127–134.

Wilk A, Szypulska-Koziarska D, Wiszniewska B, 2017 The toxicity of vanadium on gastrointestinal, urinary and reproductive system, and its influence on fertility and fetuses malformations. Postepy. Hig. Med. Dosw. (Online) 71(0), 850–859. [PubMed: 29039350]

Xia T, Kovochich M, Liong M, Mädler L, Gilbert B, Shi H, Yeh JI, Zink JI, Nel AE, 2008 Comparison of the mechanism of toxicity of zinc oxide and cerium oxide nanoparticles based on dissolution and oxidative stress properties. ACS Nano 2(10), 2121–2134. [PubMed: 19206459]

Yah CS, Simate GS, Iyuke SE, 2012 Nanoparticles toxicity and their routes of exposures. Pakistan Journal of Pharmaceutical Sciences 25(2), 477–491. [PubMed: 22459480]

Yu J, Asche CV, Fairchild CJ, 2011a The economic burden of dry eye disease in the United States: a decision tree analysis. Cornea 30(4), 379–387. [PubMed: 21045640]

Yu D, Walters DM, Zhu L, Lee PK, Chen Y, 2011b Vanadium pentoxide (V(2)O(5)) induced mucin production by airway epithelium. Am. J. Physiol. Lung Cell Mol. Physiol 301(1), L31–39. [PubMed: 21531775]

Zhou EH, Watson C, Pizzo R, Cohen J, Dang Q, Ferreira de Barros PM, Park CY, Chen C, Brain JD, Butler JP, Ruberti JW, Fredberg JJ, Demokritou P, 2014 Assessing the impact of engineered nanoparticles on wound healing using a novel in vitro bioassay. Nanomedicine (Lond) 9(18), 2803–2815. [PubMed: 24823434]

Highlights

- Zinc oxide (ZnO) and vanadium pentoxide (V_2O_5) engineered nanomaterials (ENMs) markedly decreased viability of the immortalized corneal epithelial (hTCEpi) cells.
- Low concentrations of ZnO and V_2O_5 ENMs significantly decreased migration of the hTCEpi cells.
- The ZnO and V_2O_5 ENMs showed no effects to the precorneal tear film.
- Corneal epithelial wound healing was significantly delayed by topical ZnO ENM *in vivo*.
- Both the ZnO and V_2O_5 ENMs penetrated through all corneal layers.

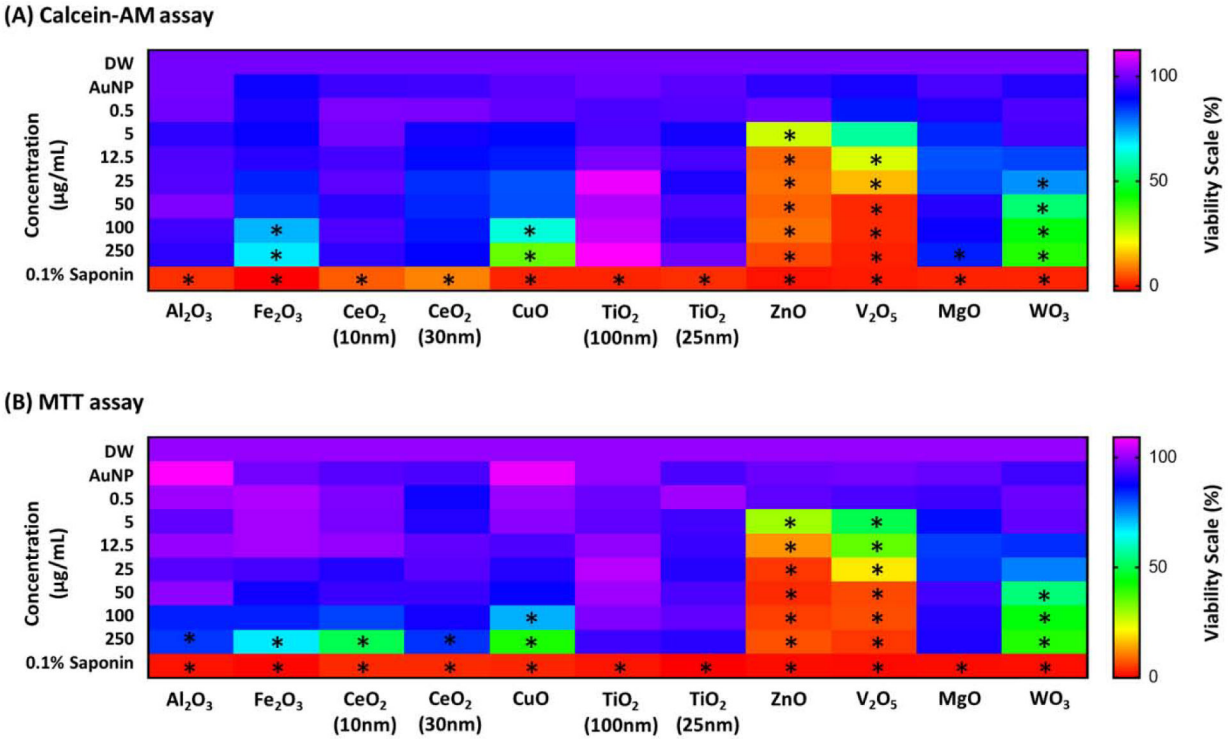

Figure 1. Corneal epithelial cell viability was markedly reduced following treatment with ZnO and V_2O_5 ENMs.

Calcein-AM (A) and MTT assays (B) revealed similar cell viability results for 11 metal oxide ENMs. The V_2O_5 nanoflakes and ZnO nanoparticles were most potent at inducing cytotoxicity in comparison to the other metal oxide ENMs. A heatmap is used to indicate cell viability with purple and red indicate a high and low percentage of hTCEpi cell viability, respectively; other colors indicate intermediate viability as detailed on the viability scale. *$P < 0.05$, Kruskal-Wallis test followed by Dunn's multiple comparisons test was performed to compare with the vehicle (DW) controls. DW, deionized water; Au NP, gold nanoparticle; Al_2O_3, aluminum oxide; Fe_2O_3, iron(III) oxide; CeO_2, cerium(IV) oxide; CuO, copper(II) oxide; TiO_2, titanium(IV) oxide; ZnO, zinc(II) oxide; V_2O_5, vanadium(V) oxide; MgO, magnesium(IV) oxide; WO_3, tungsten(VI) oxide.

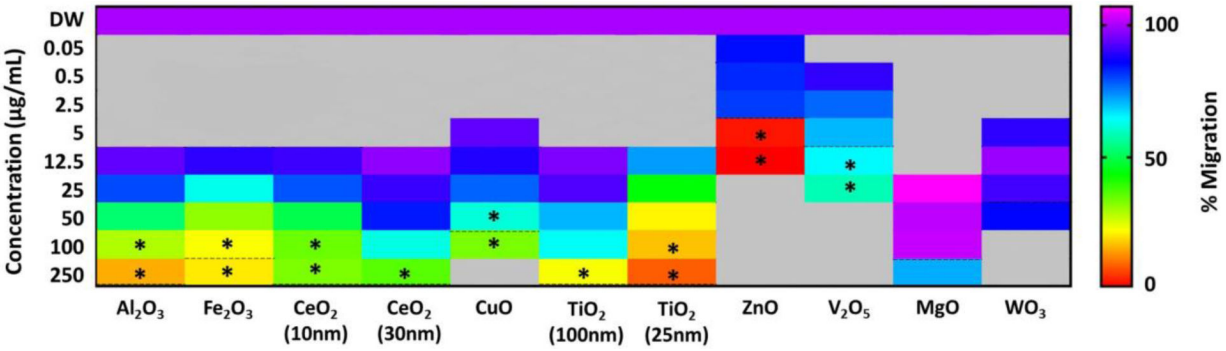

Figure 2. Corneal epithelial cell migration *in vitro* was significantly reduced by low concentrations of ZnO or V_2O_5 ENMs.

The Oris™ 96-well cell migration assay kit was used to assess cell migration *in vitro*. Compared with other metal oxide ENMs, ZnO and V_2O_5 ENMs were more potent at inhibiting cell migration. A heatmap is used to indicate cell viability with purple and red indicate a high and low percentage of hTCEpi cell viability, respectively; other colors indicate intermediate viability as detailed on the viability scale. Grey color indicates doses that were not performed based on viability data. $*P < 0.05$, Kruskal-Wallis test followed by Dunn's multiple comparisons test was performed to compare with the vehicle (DW) controls. DW, deionized water; Au NP, gold nanoparticle; Al_2O_3, aluminum oxide; Fe_2O_3, iron(III) oxide; CeO_2, cerium(IV) oxide; CuO, copper(II) oxide; TiO_2, titanium(IV) oxide; ZnO, zinc(II) oxide; V_2O_5, vanadium(V) oxide; MgO, magnesium(IV) oxide; WO_3, tungsten(VI) oxide.

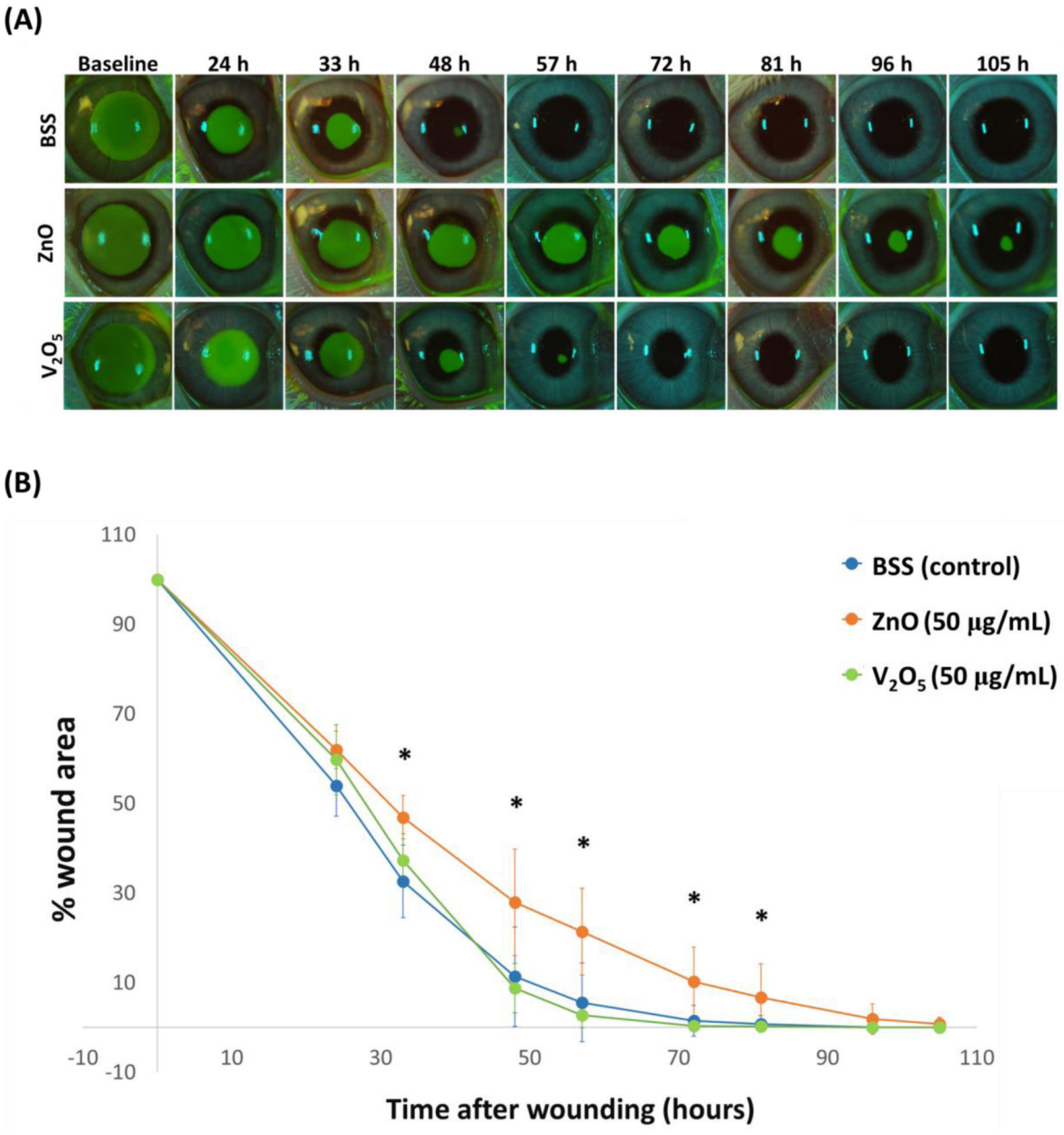

Figure 3. Topical ZnO NP but not V_2O_5 nanoflake suspensions significantly delayed epithelial wound repair in an *in vivo* rabbit model.

(A) Representative images of corneal epithelial wound healing in rabbits treated with topical ZnO NP, V_2O_5 nanoflake or BSS six times daily. (B) The ZnO treated group showed significantly delayed corneal epithelial wound healing rates from 33 to 81 hours post wounding compared with V_2O_5 treated group ($P < 0.001$ from 33 to 72 h and $P = 0.01$ at 81 h) and BSS controls ($P < 0.001$ from 33 to 72 h and $P = 0.02$ at 81 h). No significant differences were identified between V_2O_5 and BSS treated groups at all time points. *$P < 0.05$, repeated measures two-way ANOVA followed by Tukey's multiple comparisons.

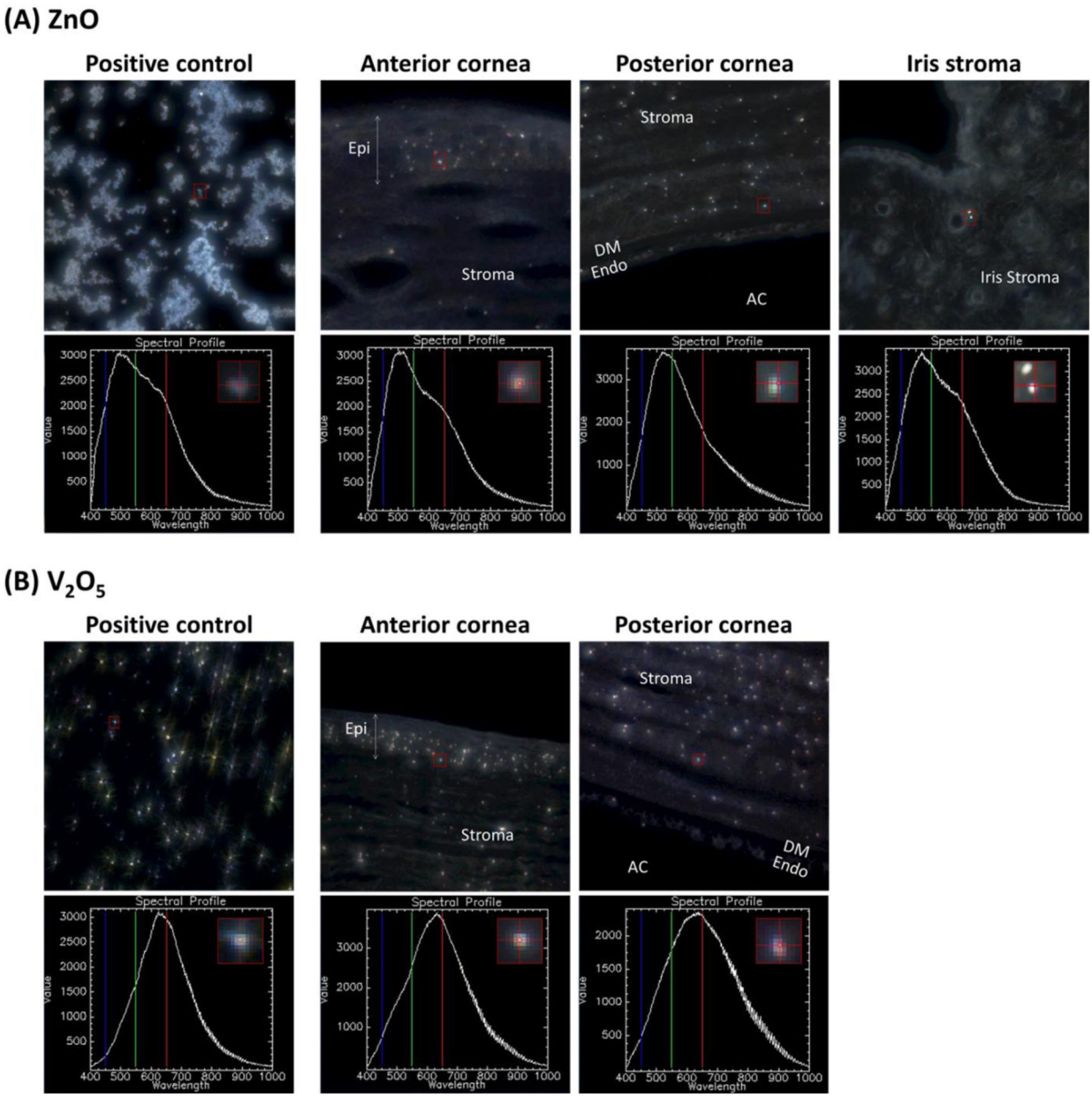

Figure 4. The ZnO and V_2O_5 ENMs accumulated in all corneal layers following topical treatment using hyperspectral darkfield microscopy in both wounded and unwounded eyes.

Both ZnO and V_2O_5 ENMs were observed in the corneal epithelium (Epi), stroma, Descemet's membrane (DM) and endothelium (Endo) while a few particles of ZnO was also observed in the iris stroma. The presented images are from wounded eyes. Epi, epithelium; DM, Descemet's membrane; Endo, endothelium; AC, anterior chamber.

Table 1.

Multiple precorneal tear film parameters were assessed prior to and following 7 days of topical treatment with ZnO or V_2O_5 ENM suspensions or vehicle control (BSS) six times daily.

Kolmogorov-Smirnov test (nonparametric t-test) was performed to compare between day 0 and 7. There are no significant differences between BSS and ZnO or V_2O_5 at any time point and no differences between ZnO and V_2O_5 at any time point.

1. Schirmer Tear Test (mm/min)			
	Day 0	**Day 7**	**P-value**
BSS	11.4 ± 3.8	8.8 ± 1.7	0.100
ZnO	9.3 ± 2.6	10.1 ± 2.5	0.847
V_2O_5	10.5 ± 3.2	11.5 ± 1.8	0.518
2. Tear Film Break-Up Time (sec)			
	Day 0	**Day 7**	**P-value**
BSS	82 ± 20	115 ± 16	0.143
ZnO	72 ± 21	79 ± 31	0.304
V_2O_5	105 ± 36	76 ± 44	0.395
3. Tear Film thickness (μm)			
	Day 0	**Day 7**	**P-value**
BSS	10.9 ± 1.2	10.9 ± 1.5	0.847
ZnO	11.4 ± 1.3	12.1 ± 3.0	0.249
V_2O_5	13.3 ± 2.0	13.6 ± 1.9	0.996
4. Tear meniscus height (μm)			
	Day 0	**Day 7**	**P-value**
BSS	0.031 ± 0.012	0.027 ± 0.009	0.518
ZnO	0.035 ± 0.014	0.027 ± 0.008	0.146
V_2O_5	0.031 ± 0.014	0.046 ± 0.022	0.249
5. Tear meniscus length (μm)			
	Day 0	**Day 7**	**P-value**
BSS	249 ± 54.2	218 ± 39.0	0.249
ZnO	250 ± 50.8	222 ± 27.9	0.159
V_2O_5	241 ± 54.7	300 ± 91.7	0.518
6. Tear meniscus area (mm^2)			
	Day 0	**Day 7**	**P-value**
BSS	0.032 ± 0.012	0.026 ± 0.010	0.996
ZnO	0.036 ± 0.015	0.027 ± 0.008	0.866
V_2O_5	0.032 ± 0.014	0.046 ± 0.023	0.847